Key Points:
- Primary production in East Antarctic fast and pack sea ice is not Fe-limited during summer
- Low nitrate and high exopolysaccharide concentrations suggest heterotrophic dominance in Antarctic summer sea ice
- Fe-rich platelet sea ice near the Moscow University Ice Shelf indicates an influence of glacial meltwater in the coastal distribution of Fe

Nutrient Distribution in East Antarctic Summer Sea Ice: A Potential Iron Contribution From Glacial Basal Melt

L. Duprat[1] , M. Corkill[1] , C. Genovese[1] , A. T. Townsend[2] , S. Moreau[3] , K. M. Meiners[4,5] , and D. Lannuzel[1]

[1]Institute for Marine and Antarctic Studies, University of Tasmania, Hobart, TAS, Australia, [2]Central Science Laboratory, University of Tasmania, Hobart, TAS, Australia, [3]Norwegian Polar Institute, Tromsø, Norway, [4]Department of Agriculture, Water and the Environment, Australian Antarctic Division, Kingston, TAS, Australia, [5]Australian Antarctic Program Partnership, Institute for Marine and Antarctic Studies, University of Tasmania, Hobart, TAS, Australia

Abstract Antarctic sea ice can incorporate high levels of iron (Fe) during its formation and has been suggested as an important source of this essential micronutrient to Southern Ocean surface waters during the melt season. Over the last decade, a limited number of studies have quantified the Fe pool in Antarctic sea ice, with a focus on late winter and spring. Here we study the distribution of operationally defined dissolved and particulate Fe from nine sites sampled between Wilkes Land and King George V Land during austral summer 2016/2017. Results point toward a net heterotrophic sea-ice community, consistent with the observed nitrate limitation (<1 μM). We postulate that the recycling of the high particulate Fe pool in summer sea ice supplies sufficient (~3 nM) levels of dissolved Fe to sustain ice algal growth. The remineralization of particulate Fe is likely favored by high concentrations of exopolysaccharides (113–16,290 μg xeq L^{-1}) which can serve as a hotspot for bacterial activity. Finally, results indicate a potential relationship between glacial meltwater discharged from the Moscow University Ice Shelf and the occurrence of Fe-rich (~4.3 μM) platelet ice in its vicinity. As climate change is expected to result in enhanced Fe-rich glacial discharge and changes in summer sea-ice extent and quality, the processes influencing Fe distribution in sea ice that persists into summer need to be better constrained.

Plain Language Summary Iron (Fe) plays a crucial role in microalgal physiology and can control their growth in the Southern Ocean, where Fe concentrations are naturally low. Antarctic sea ice can incorporate high levels of Fe during its formation triggering phytoplankton blooms at the sea-ice edge during the melt season. No studies to date have assessed sea-ice Fe distributions in East Antarctica during mid- to late summer. Here we discuss Fe distribution in parallel with key sea-ice physical and biological parameters measured during an expedition to East Antarctica in summer 2016/2017 to answer our central question: is Fe limiting sea-ice primary productivity during summer? Results suggest nitrate, rather than Fe is the key nutrient controlling sea-ice algal growth at this time of the year. We also found Fe-rich platelet ice incorporated underneath pack ice sampled near the Moscow University Ice Shelf which suggests the potential accretion of Fe-rich ice shelf waters under the sea ice. As climate change is expected to accelerate Antarctic ice shelve melting, a better understanding of how increased rates of glacial meltwater discharge will impact the distribution of Fe within the sea ice during summer is needed.

1. Introduction

Phytoplankton growth can be limited by the availability of the essential nutrient iron (Fe; Baar et al., 1990, 1995). The Southern Ocean (SO) is a classic example where high concentrations of macronutrients (nitrate, phosphate, and silicic acid) do not support the expected level of primary production due to low Fe concentrations. The SO has therefore been designated as a High Nutrient Low Chlorophyll (HNLC) area (Martin, 1990). In this context, sea ice plays a pivotal role as a natural and biogeochemically active Fe reservoir due to the high levels of Fe and organic matter concentrated from seawater during its formation (Gradinger & Ikavalko, 1998; Janssens et al., 2016; Lannuzel et al., 2007, 2016). As the sea ice begins to melt in spring, this Fe pool can sustain concentrated algal blooms at the retreating sea-ice edges and in opening polynyas, contributing to the spatial variability in SO primary production (Arrigo 1998; Lancelot et al., 2009; Lannuzel et al., 2007, 2008; Massom & Stammerjohn, 2010; Sedwick et al., 1997). This process can alleviate

Fe limitation at a critical time, when light availability and water stratification favor phytoplankton growth, making Antarctic sea ice an important natural Fe fertilizer in the SO (Tagliabue & Arrigo, 2006).

The availability of light can co-limit (with Fe) sea-ice primary productivity for the vast majority of the year (Thomas & Dieckmann, 2010). The distribution of solar radiation has major impacts on sea-ice physical and biological processes (Arrigo et al., 2012). Snow thickness is usually the most important factor regulating the availability of light for ice algae because of its high light attenuation properties (Arrigo et al., 1998). However, snow metamorphosis during summer can reduce this attenuation (Arndt et al., 2017; Haas et al., 2001; Hancke et al., 2018; Tison et al., 2008). Within nonflooded areas, the melting coarse-grained summer snowpack has a lower albedo than the cold fine-grained snow, allowing more light to pass through the snow (Brandt et al., 2005; Zhou et al., 2007). More important, enhanced areas of surface flooding in Antarctic summer sea ice can significantly reduce light attenuation (Arndt et al., 2017; Arrigo et al., 2012). On a larger scale, the common presence of features of higher light transmittance in summer sea ice, such as leads and cracks, should increase the lateral incidence of light (Katlein et al., 2015). Summer ice features associated with low salinity extremes, such as melt ponds, under ice melt lenses, and rotten ice, most likely select for microalgal species capable of tolerating these extremes as well (Torstensson et al., 2018). These observations corroborate with a previous modeling study showing that nutrients rather than light or salinity, limit Antarctic sea-ice algae growth during summer (Saenz & Arrigo, 2014).

A high percentage of sea-ice dissolved Fe (DFe, filtered through a 0.2 μm pore size membrane), our best empirical measurement of potentially bioavailable Fe (Morel et al., 2008), is lost to the seawater in a rapid pulse over a few days during spring (Duprat et al., 2019; Lannuzel et al., 2008). This early release is likely rapidly consumed by phytoplankton with very low DFe concentrations reported for seawater after the spring bloom (Bertrand et al., 2011; Sedwick et al., 2000, 2011). Sea-ice melt may provide an additional later pulse of Fe to surface waters in the particulate form (PFe, > 0.2 μm), as the flushing of this pool from the sea ice is initially limited by brine channel transport (Lannuzel et al., 2013; van der Merwe et al., 2011). Studies conducted during the last two decades indicate that sea-ice DFe concentrations are relatively unaffected by the proximity to Fe sources (Lannuzel et al., 2016, and references therein). This apparent contradiction has been attributed to the fact that in the presence of saturated organic ligands, the dissolution equilibrium should impose a maximum threshold for DFe concentrations in sea ice. When all organic ligands are saturated, excess DFe precipitates into PFe. Much of East Antarctica's free-floating pack ice is formed in leads and polynyas (Allison, 1989), and due to an increased distance to coastal sources, it generally carries a lower concentration of lithogenic PFe than land-fast sea ice (sea ice fastened to coastal features; Lannuzel et al., 2016). The accumulation of PFe in pack ice can still occur, either by uptake and conversion of DFe (e.g., from the continental shelf or icebergs) into PFe, or via direct incorporation of biogenic PFe from highly productive shelf waters where it originated (Lannuzel et al., 2016).

In contrast to pack ice, fast ice can be affected by a greater input of Fe from lithogenic sources, such as coastal sediment (de Jong et al., 2012) and dust from ice-free continental areas (de Jong et al., 2013; Duprat et al., 2019). Less clear is the influence of subglacial meltwater on the fast-ice Fe pool via incorporation of ice platelets at the bottom of sea ice. The growth of ice platelets has been observed below sea ice under the influence of ice-shelf meltwater (Langhorne et al., 2015). There are several observations of platelet ice in the Ross and Weddell seas; otherwise, there are very few reports of platelet ice layers in East Antarctica (Langhorne et al., 2015). It is believed they are seeded by frazil crystals formed in supercooled ice shelf waters, although the processes behind the formation of these unique crystallographic structures are still poorly understood (Tison et al., 1998). The ice platelets can eventually be incorporated onto the base of the ice shelf (marine ice) via buoyant accumulation (Oerter et al., 1992), or be carried out from the ice shelf cavity and deposited beneath neighboring sea ice (subice platelet layers; Langhorne et al., 2015; Tison et al., 1998). Under sea ice, in-situ growth can continue, creating a porous and friable subice platelet layer from which the highest concentrations of sea-ice algae (up to 374 mg C L^{-1} and 6.5 mg Chl$a$ L^{-1}) have been reported (Arrigo et al., 2010; Bombosch, 2013; Smetacek et al., 1992; van der Linden et al., 2020). The origin of marine ice Fe is often associated with highly reactive glacial flour produced from subglacial physical and chemical weathering (Wadham et al., 2010). The presence of buoyant frazil and ice platelets could facilitate the incorporation of sediment and biogenic material from the ocean into the marine ice layer (Treverrow et al., 2010). While platelet ice incorporation under ice shelves has been associated with higher concentrations of Fe
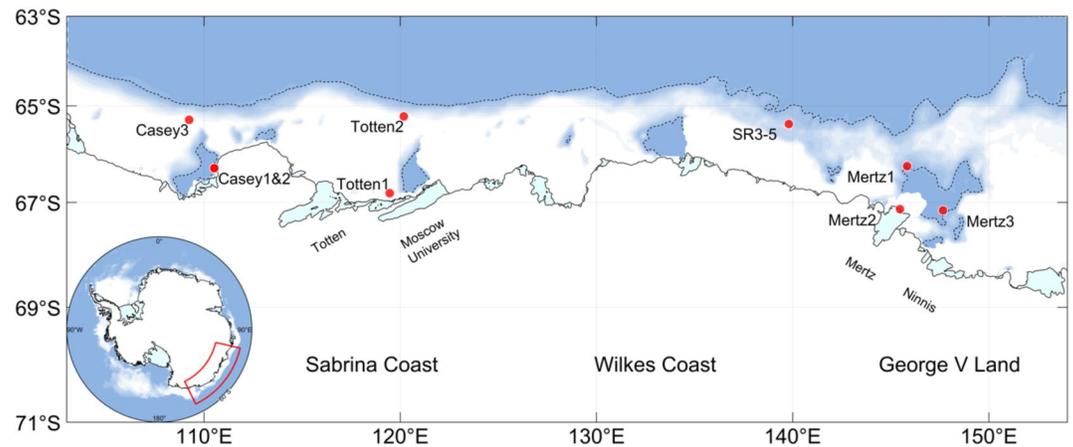
Figure 1. Map with the locations and names of sea-ice stations off East Antarctica visited between December 19, 2016 and January 13, 2017 during the Research Survey Vessel (RSV) Aurora Australis Voyage 2. Sea-ice concentration averaged for the study period is shown by a gradient between blue (low) and white (high). Major ice shelves (Totten, Moscow University, Mertz and Ninnis) are also labeled.

(Herraiz-Borreguero et al., 2016), no link has yet been made for platelet ice incorporation under sea ice due to the paucity of observations and measurements.

To date, most sea-ice surveys focused on investigating Fe distribution and biogeochemistry in late winter and spring (Lannuzel et al., 2016). In this study, we report Fe concentrations obtained from between Wilkes Land and King George V Land coast (East Antarctica) and sampled during a marine science voyage carried out from December 2016 to January 2017. We aim to answer our central question: is sea-ice primary production Fe-limited in summer due to the advanced stage of brine and nutrient drainage? A further objective was to evaluate how the Fe biogeochemistry relates to macronutrients and other biological variables in summer sea ice, such as algae-produced exopolysaccharides (EPS). The final aim of this study was to investigate a potential link between glacial basal melt from ice shelves encountered during our expedition (e.g., Moscow University, Mertz and Ninnis) and the formation of Fe-rich platelet ice, as an important spatial determinant in sea-ice PFe distribution. Results from this study could guide studies on the potential impacts of future ice mass balance changes on local primary production, and carbon export of highly productive polynyas found downstream of the Dalton, Mertz and Ninnis ice shelves (Paolo et al., 2015; Rignot et al., 2019).

2. Methods

2.1. Sampling Sites

Sea ice was sampled during an icebreaker *Research Survey Vessel Aurora Australis* voyage at nine different stations off the East Antarctic coast (Figure 1) during austral summer (December 2016 to January 2017). The mobility of the ice stations (e.g., fastened vs. free-floating) was used as criteria to categorize the stations into fast and pack ice (see Section 3.1). Casey 1 and 2 were fast ice stations on first-year ice in O'Brien Bay near Casey Station (~5 km). Exposed rocky hills surrounded the site. Totten 1 was sampled ~15 km from the Moscow University Ice Shelf and ~75 km from the Totten Ice Shelf. Pack ice stations were diverse: Casey 3 and Totten 2 consisted of thick rafted ice with a very uneven surface, while SR3-5, Mertz 1, 2, and 3 were relatively level ice floes. Mertz 1, 2, and 3 stations were approximately 95, 1, and 75 km from the Mertz Glacier Tongue, respectively. Snow depths were variable, and most snow was old and compacted. Sampling sites were selected away and upwind from the research vessel or any other operations likely to contaminate trace metal and organic matter samples.

2.2. Cleaning Procedures

Plasticware used for sample collection (polypropylene [PP; Superlift®] melting containers) and storage (low-density polyethylene [LDPE; Nalgene®] sampling bottles) were kept in sealed plastic bags after being acid-cleaned according to GEOTRACES recommendations. First, new LDPE bottles were soaked in 2% (v:v) Decon90 baths for 1 week. Bottles were then thoroughly rinsed with ultra-high purity water (UHP water, Barnstead), filled with 6 M hydrochloric acid (HCl, 50% v:v reagent grade, Merck) and immersed in 2 M HCl (~20% v:v reagent grade, Merck) for one month. Bottles were then rinsed with UHP water, filled with 1 M distilled HCl (~10% v:v instrument quality, Seastar) and kept for 1 week on a hot plate (60°C). Finally, bottles were rinsed three times with UHP water in a class-100 laminar flow hood and stored triple bagged in plastic press seal bags until use. Between sampling days, plastic equipment (Teflon® filtration sets, plastic tubing, and plastic scoops) used for collection and processing were rinsed with UHP water and soaked in an acid bath (10%–20% v:v HCl, according to Nalgene® recommendations for each material) and thoroughly rinsed again with UHP water before use. Finally, glassware used for organic carbon and nitrogen filtrations were soaked in a 2% (v:v) HCl solution (reagent grade, Merck), rinsed with UHP water, wrapped in aluminum foil, and combusted at 450°C for 4 h.

2.3. Sampling Procedures

During field sampling, trace metal clean protocols were followed, as described by Lannuzel et al. (2006) and van der Merwe et al. (2009). The snow was collected using an acid-cleaned polyethylene (PE) hand shovel and stored in a 3.8 L wide-mouth Nalgene® high-density polyethylene (HDPE) bottle. Separate cores from the same vicinity were collected for temperature/salinity, particulate organic matter (POM), chlorophyll-a (Chl$a$), particulate EPS (PEPS), macronutrient and Fe determinations. Ice cores were collected with an electric-powered, electro-polished stainless-steel corer of 0.14 m internal diameter (Lichtert Industrie, Belgium), previously shown appropriated for trace metal sampling (Lannuzel et al., 2006; van der Merwe et al., 2009). Ice cores were sectioned in the field using a medical-grade bone saw (Richards Analytical). Six or seven sections were obtained out of the entire core (from top, intermediate, and bottom layers), 10–15 cm thick, in order to represent different depth horizons of the ice cores. Snow and sea-ice samples were melted at room temperature immediately after collection, filtered (for the dissolved fraction, see details in paragraph 2.4.2) and poured into 125 mL Superlift® PP bottles, double bagged and stored at −20°C until analysis. Brine was collected from ~1 m deep sack holes, while underlying seawater was collected through full-ice-depth core holes, just below the ice (hereafter referred to as SW0m). Both brine and seawater were collected using an acid-cleaned 0.5 L perfluoroalkoxy (PFA) bottle (Nalgene®) attached to an improvised 2 m long bamboo pole and transferred into acid-cleaned 1L LDPE bottles (Nalgene®).

2.4. Sample Processing and Analytical Methods

2.4.1. Physical Variables

Sea-ice temperatures were measured with a Testotherm720 thermometer (accuracy ± 0.1°C) immediately after ice core retrieval from small holes drilled in the core at 0.1 m intervals. Bulk salinities of brine, seawater, melted snow, and sea-ice sections were measured using a Guildline Autosal salinometer (Ocean Scientific International Ltd, UK; ± 0.001 practical salinity unit [PSU]). The texture of each ice core was analyzed by photographing vertical thin sections between cross-polarizing filters, following the method of Langway (1958). The physical ice properties are discussed in more detail in a companion paper. Finally, a light sensor was deployed in the core hole to measure the luminous ice emittance (per square meter) at 0.1 m increments as an indication of the light intensity that passed through different depth horizons of the sea ice.

2.4.2. Fe Physical Fractionation

Dissolved and particulate Fe from snow, seawater, brine, and melted sea-ice sections were obtained by filtration through 0.2 μm pore size 47 mm diameter polycarbonate (PC) membrane filters (Sterlitech) using Teflon® PFA filtration apparatus (Savillex, USA). A gentle vacuum (<0.13 bar) was applied to avoid algal

cell rupture during filtration. The dissolved fraction (<0.2 µm, which includes the soluble (<0.02 µm) and colloidal (0.02–0.2 µm) fractions) was collected in LDPE bottles, acidified to pH 1.8 by adding ~1% (v:v) of 12 M ultrapure HCl (Seastar Baseline, analytical grade), triple-bagged and stored at room temperature until analysis. PC filters with the retained particulate fraction (>0.2 µm) were placed into acid-clean polystyrene Petri dishes, triple-bagged, and stored at −20°C in the dark until further processing and analysis at the University of Tasmania (Australia).

2.4.2.1. DFe Analysis

An automated off-line sample system (seaFAST-pico™, Elemental Scientific; Nobias Chelate-PA1 resin) was used to preconcentrate trace metals and remove sea-ice and seawater filtrate matrices from our samples according to the method described by Wuttig et al. (2019). Comprehensive method testing using a variety of internationally recognized community reference samples and oceanographic standards (Wuttig et al., 2019) as well as NASS-6 verified method accuracy for Fe. A mean Fe value of 9.24 ± 0.24 nmol kg^{-1} ($n = 6$) was measured for the NASS-6, in good agreement with the reported indicative value of 8.65 ± 0.81 nmol kg^{-1}. Collected samples were concentrated either 10× (bottom sections of sea ice and brines) or 40× (snow, remaining sections of sea ice, and seawater) depending on the expected Fe concentrations. DFe concentrations were then determined using a Sector Field Inductively Coupled Plasma Mass Spectrometer (SF-ICP-MS, Element 2; Central Science Laboratory [CSL], University of Tasmania). Cleaning procedures, calibrations and quality control of the SF-ICP-MS results for the samples analyzed in this study followed those described in Duprat et al. (2019). The average detection limit for DFe was calculated as 7.8×10^{-4} ppb (0.014 nM; $n = 15$; 3× the standard deviation of the acidified internal blank). Concentrations reported here are all blank corrected. Finally, Fe* was calculated as a way to assess potential Fe deficiency relative to PO_4^{3-}. Fe* was estimated by subtracting the biological contribution based on the Fe:PO_4^{3-} assimilation ratio (0.47 mmol:mol), following Parekh et al. (2005).

2.4.2.2. Particulate Fe

Particulate Fe was quantified after complete filter digestion using a strong acid treatment (Bowie et al., 2010). First, a mixture of 250 µL 12 M HCl, 250 µL 16 M nitric acid (HNO$_3$, SeaStar Baseline), and 500 µL 29 M hydrofluoric acid (Seastar Baseline, Choice Analytical) was added to each sample and blank filter and placed into a Teflon® PFA vial (Savillex, USA). Vials were heated to 120°C for 12 h over a Teflon® coated hotplate (SCP Science) housed within a class-100 fume hood. Vials were then left open until complete evaporation of the acids. Next, 9.9 mL of ultrapure 10% (v:v) HNO$_3$ was added to re-suspend the dried residues before the addition of 100 µL Indium solution (final concentration 87.1 nM) as an internal standard. Finally, an aliquot of 5 mL was transferred to PP tubes for Fe quantification using SF-ICP-MS following similar procedures as outlined in Section 2.4.2.1. The detection limit for Fe was calculated as 3× the standard deviation of the digested acid filter blank, determined as 8×10^{-4} ppb (0.14 nM). The theoretical biogenic fraction (PFe$_{bio}$) was calculated as the total PFe—lithogenic PFe (inferred by the Fe:Al ratio of 0.33; Taylor & McLennan, 1985). It is worth noting that Fe enrichment relatively to Al can occur via flocculation and increasing sorting of lithogenic material with distance from the coast (Markussen et al., 2016), therefore results should be interpreted with care. For the purpose of this work, we refer to biogenic Fe as any PFe form associated to biogenic pools (living, detrital, and authigenic) that are not refractory particles originated from terrestrial sources of rock, such as silicate minerals (lithogenic origin).

2.4.3. Particulate Organic Matter

Melted sea-ice and seawater samples for particulate organic matter determination were gently homogenized before filtration (0.14–0.6 L) on precombusted (450°C, for 8 h) glass microfiber (GF/F) filters (0.7 µm nominal porosity, MGF Sartorius). Samples were dried overnight at 60°C. Inorganic carbon contamination was removed from the filters with the addition of 10% (v:v) distilled HCl (80 µL) for 12 h inside a closed PCR well tray (Martin, 1993). Samples were then packed in silver cups (Elemental Microanalysis, UK) and stored in a desiccator until analysis for elemental composition at the CSL. Particulate organic carbon (POC) and

particulate organic nitrogen (PON) concentrations were determined by flash combustion and oxygen pyrolysis using a Thermo Finnigan EA 1112 Series Flash Elemental Analyzer (estimated precision ~1%). POC and PON detection limits were calculated as 3× the standard deviation of the procedure blanks, determined as 2.5 and 1.8 μM, respectively ($n = 6$).

2.4.4. Particulate EPS

In aquatic systems, dissolved EPS are prone to coalesce into particulate form, also referred to PEPS. Sea-ice, brine, and seawater PEPS concentrations were measured using the semi-quantitative colorimetric Alcian Blue assay (Passow & Alldredge, 1994) following van der Merwe et al. (2009). Calibration was achieved by measuring five different extracted solutions from filters previously treated with 0, 2.5, 5, 7.5, and 10 mL of a 0.75 μg L^{-1} Xanthan gum solution, following the same staining protocol used for the sample filters. A linear regression ($R^2 = 0.92$; $n = 16$) was calculated between absorbance and the respective concentration of Xanthan gum. The detection limit (3× the standard deviation of the filter blank) was 28.6 μg Xanthan equivalent (xeq.) L^{-1} ($n = 20$).

2.4.5. Chl*a* and Macronutrients

Samples for Chl*a* analysis were melted at room temperature in the dark (Rintala et al., 2014). Chlorophyll *a* was concentrated by filtering samples (0.09–0.7 L) through GF/F filters under low vacuum (<0.13 bar) followed by extraction with 90% acetone (High Performance Liquid Chromatography grade) for 12–24 h. Chlorophyll *a* concentrations were determined fluorometrically with a Turner Designs 10AU fluorometer (in vitro detection limit 0.02 μg L^{-1}). Fluorescence was measured at 750 nm before and after acidification with 0.1 M HCl, and phaeopigment-corrected Chl*a* was calculated according to Arar and Collins (1997). Macronutrient samples were collected via filtration over 0.2 μm pore size filters (Acrodiscs) placed inside a filter holder and stored frozen (−20°C) in 60 mL HDPE bottles until analysis in the laboratory (CSIRO, Hobart, Australia). Concentrations of nitrate + nitrite (NO*x*), nitrite (NO$_2^-$), ammonium (NH$_4^+$), phosphate (PO$_4^{3-}$), and (ortho)silicic acid (Si(OH)$_4$) were determined using a segmented flow analyzer (SEAL Analytical Ltd AA3 HR Autoanalyzer) following standard colorimetric methods from Rees et al. (2018), and Kérouel and Aminot (1997) for NH$_4^+$. Salinity-normalized macronutrient concentrations (C*) were calculated to tease apart physical effects following the equation applied by Fripiat et al. (2017): C* = $C \cdot (S_w/S)$, where C is the measured nutrient concentration in the bulk sea ice, S_w is the salinity of seawater and S the corresponding measured salinity of in the bulk ice sample.

2.5. Statistical Analysis

Distributions of variables were tested from all stations and within both the pack and fast ice groups. First, the normality and the homogeneity of variance of each variable was tested using the Shapiro-Wilk test and Levene's test, respectively. When the normality and homogeneity of variance could be verified, an analysis of variance test was run. For non-normal distributed variables, the Kruskall-Wallis test was used. Multiple (paired) comparisons corrected by the Holm test were performed. Differences between fast and pack ice were also tested using either a Wilcoxon test or a *t*-test, depending on the distribution. Potential correlations between all physical and biogeochemical parameters were investigated using a Spearman correlation coefficient test due to the non-normality observed in most variables. For this test, ice texture proportions were calculated for each section using rankings 0 for noncolumnar (granular and platelet) and 1 for columnar. All analyses were performed using the R programming language (version 3.3.1; R Core Team, 2013).

Table 1
Sampling Dates, Location, and General Characteristic/Texture of Ice Stations

| Station | Date of sampling (2016/2017) | Location | | General floe description/texture |
		Latitude (°N)	Longitude (°E)	
Casey 1	December 19, 2016	−66.3 S	110.5 E	
Casey 2	December 23, 2016	−66.3 S	110.5 E	Fast ice/no texture data
Casey 3	December 27, 2016	−65.3 S	109.2 E	Thick rafted pack ice with gap/no texture data
Totten 1	December 31, 2016	−66.8 S	119.5 E	Ex-fast ice/superimposed ice, snow ice, layers of columnar and granular ice, platelet ice
Totten 2	January 03, 2017	−63.2 S	120.2 E	Thick rafted pack ice/no texture data
SR3-5	January 07, 2017	−63.4 S	139.8 E	Rafted pack ice with gap/superimposed ice, snow ice, granular ice
Mertz 1	January 09, 2017	−66.3 S	145.8 E	Pack ice/superimposed ice, snow ice, layers of granular and columnar ice including a layer of platelet ice
Mertz 2	January 11, 2017	−67.1 S	145.5 E	Pack ice/superimposed ice, snow ice, granular ice, platelet ice
Mertz 3	January 13, 2017	−67.2 S	147.7 E	Surface flooded pack ice/No texture data

3. Results

3.1. Ice Physics

All collected ice cores were relatively warm (>−2°C). Porosities were almost always above the percolation threshold of 5% for columnar ice and often greater than 10%, which likely allowed brine movement through the more random brine inclusions of granular ice found in the ice cores. Brines were stratified, indicating exchange with the underlying seawater was limited to diffusive processes. The overall low brine salinities (0.9–32.2 PSU) were indicative of surface-melt input which was likely driving desalination. Of the textures sampled near ice shelves, columnar ice was often interspersed with layers of granular ice or platelet ice. Granular ice was found near the surface, especially as snow ice, while platelet ice was found at greater depths, beyond ∼0.5 m (Totten and Mertz) and beyond ∼1 m in one instance in front of the Mertz Glacier Tongue (Table 1). Measured illuminance reached optimum diatom growth values (1,000 lx; Azam & Singh, 2013) at the ice ∼0.4 m depth. Average depth-adjusted illuminance varied from 2,730 lx at the ice surface to only 17 lx in basal ice.

3.2. Distribution of Fe

Dissolved and particulate Fe concentrations measured in the snow, sea ice, brine and seawater are summarized in Table 2. A detailed description of values for each station and ice section is available via the link in Section 6. The vertical DFe and PFe profiles for fast and pack ice show no clear pattern for most stations (Figure 2). DFe was enriched in sea ice relative to concurrent seawater (SW0m) and to values found in winter seawater (Figure 3a; van der Merwe et al., 2009). Concentration of PFe were up to an order of magnitude higher than the seawater below. The average concentrations of DFe and PFe for all pack and fast ice stations were 2.9 ± 1.9 nM and 323 ± 606 nM, respectively. The particulate fraction comprised 98% of the total Fe pool with average PFe:PAl ratios of 0.6 for fast ice and 1.0 for pack ice. Lithogenic PFe inferred from the ice PFe:PAl ratios represented approximately 70% in fast ice and 40% in pack ice. Fast ice showed significantly higher concentrations of DFe and PFe (4.7 ± 2.3 nM; 665 ± 980 nM) compared to pack ice (2.0 ± 0.7; 81.7 ± 48.2; $p < 0.01$). Totten 1 showed significantly higher DFe and PFe ($p < 0.01$) than the other fast ice stations. Higher DFe and PFe were also found in fast ice (3.5 ± 3.4 nM; ± 99.6 ± 64.3 nM) compared to pack ice (2.0 ± 1.3 nM; 83.2 ± 124 nM) when Totten 1 was treated as an outlier, albeit not statistically significant.

Table 2
Summary Statistics for all Biogeochemical Parameters

	DFe (nM)	PFe (nM)	NOx (μM)	NH$_4$ (μM)	PO$_4^{3-}$ (μM)	Si(OH)$_4$ (μM)	Chl$a$ (μg L^{-1})	POC (μM)	PON (μM)	POC: PON (μM:μM)	PEPS (μg xeq L^{-1})
					Fast ice						
Snow	5.7 ± 7.1	112 ± 43.8									
Sea ice											
Min.	0.7	28.5	0.1	<dl	<dl	<dl	0.1	18.6	1.4	8.8	195
Max.	13.3	4,750	4.9	2.5	5.6	16.0	92.3	285	25.3	19.8	16,290
Mean ± S.D.	4.7 ± 2.3	665 ± 980	0.7 ± 0.5	0.4 ± 0.2	0.6 ± 0.5	0.6 ± 0.5	13.3 ± 29.6	79.3 ± 15.7	6.1 ± 0.2	13.9 ± 1.6	2,540 ± 1,290
SW0m	5.3 ± 3.4	30.1 ± 18.2	2.3 ± 2.1	0.3 ± 0.1	0.3 ± 0.2	16.9 ± 13.2	9.3 ± 12.9	36.6 ± 32.1	3.9 ± 2.2	8.8 ± 4.1	1,280 ± 861
					Pack ice						
Snow	0.8 ± 0.9	27.4 ± 22.1									
Sea ice											
Min.	0.6	8.7	<dl	0.1	<dl	<dl	0.1	4.1	0.7	4.1	113
Max.	7.3	552	9.5	1.1	2.0	15.1	67.7	270	31.2	26.6	10,440
Mean ± S.D.	2.0 ± 0.7	81.7 ± 48.2	1.3 ± 2.5	0.2 ± 0.1	0.4 ± 0.4	2.7 ± 2.3	13.4 ± 18.0	70.4 ± 33.0	5.8 ± 3.4	12.8 ± 4.5	1,750 ± 720
Deep brine	1.9 ± 0.4	37.9 ± 38.4	4.9 ± 6.1	0.2 ± 0.1	0.4 ± 0.4	21.7 ± 16.9	2.3 ± 2.6	29.0 ± 14.8	4.0 ± 2.6	7.8 ± 1.8	854 ± 442
SW0m	5.7 ± 8.0	33.2 ± 56.5	15.6 ± 8.5	0.3 ± 0.2	1.1 ± 0.5	39.5 ± 15.4	2.9 ± 3.9	19.7 ± 14.6	2.7 ± 2.0	8.4 ± 6.4	377 ± 199
					All stations						
Snow	2.6 ± 4.6	63.5 ± 53.9									
Sea ice											
Min.	0.6	8.7	<dl	<dl	<dl	<dl	0.1	4.1	0.7	5.9	113
Max.	13.3	4,750	9.5	2.5	5.6	16.0	92.3	285	31.2	26.6	16,290
Mean ± S.D.	2.6 ± 4.6	2.6 ± 4.6	1.2 ± 2.4	0.3 ± 0.4	0.4 ± 0.9	2.7 ± 2.1	13.4 ± 22.1	73.3 ± 27.6	5.9 ± 2.7	13.2 ± 3.7	2,010 ± 947
SW0m	2.9 ± 1.9	2.9 ± 1.9	12.4 ± 8.6	0.4 ± 0.3	0.9 ± 0.5	31.0 ± 18.0	2.9 ± 2.8	20.6 ± 12.5	2.8 ± 1.7	7.9 ± 4.9	454 ± 223

Abbreviations: DFe, dissolved Fe; PEPS, particulate exopolysaccharides; PON, particulate organic nitrogen; POC, particulate organic carbon.
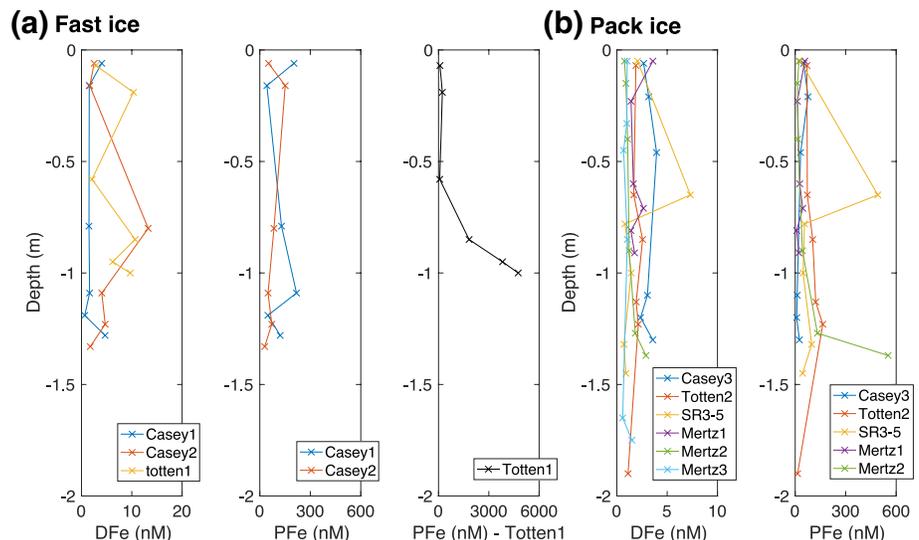

Figure 2. Vertical profiles of dissolved and particulate Fe for fast (a) and pack (b) ice stations. Different scales are used to reflect the variable concentrations. DFe, dissolved Fe; PFe, particulate Fe
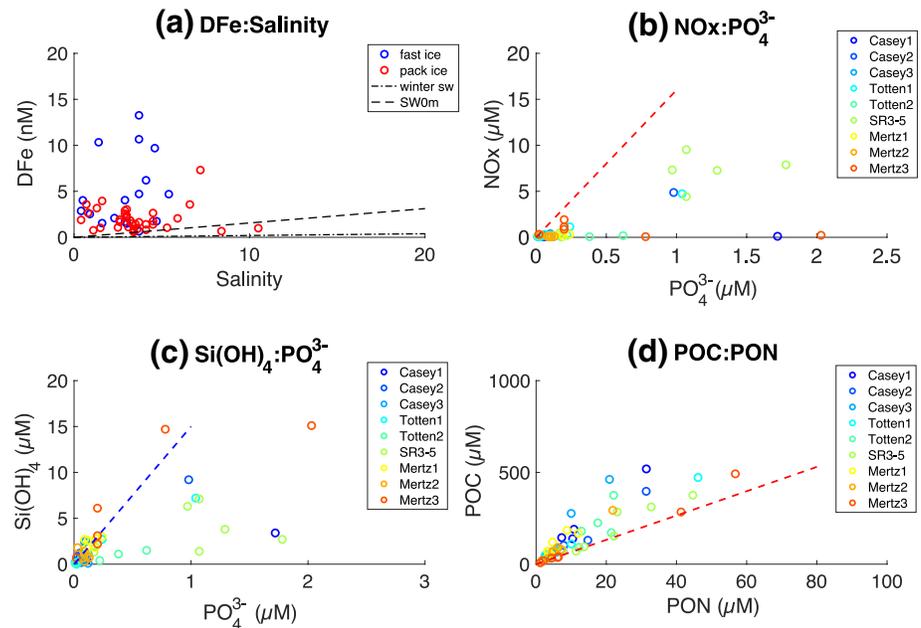
Figure 3. Relationship between biogeochemical parameters within sea ice: (a) DFe (nM) versus salinity. Dashed black line represents the theoretical dilution line (TDL) obtained from SW0m Fe and salinity values. For comparison, dash-dotted black line represents the theoretical dilution line obtained from winter-spring transition (0–1 m) seawater from East Antarctic (van der Merwe et al., 2009), (b) NO_x (NO_3^- + NO_2^-) versus PO_4^{3-} (μM:μM), (c) $Si(OH)_4$ versus PO_4^{3-} (μM:μM), (d) POC versus PON (μM:μM). Dashed red (b) and (d) and blue line (c) represent the Redfield-Brzezinski nutrient ratio (Brzezinski, 1985). DFe, dissolved Fe; POC, particulate organic carbon; PON, particulate organic nitrogen

3.3. Distribution of Macronutrients

Average concentrations of NO_x (NO_3^- + NO_2^-), PO_4^{3-}, $Si(OH)_4$ and NH_4^+ for fast and pack ice are shown in Table 2. Overall, lower concentrations of all macronutrients were found in our summer ice samples compared to other seasons (Fripiat et al., 2017). Nitrate was depleted relative to the Redfield N:P ratio (Figure 3b; Redfield, 1963). With exception of station SR3-5 and bottom ice data, $Si(OH)_4$ followed the Redfield-Brzezinski ratio for PO_4^{3-} relatively closely (Figure 3c; Brzezinski, 1985). Station SR3-5 presented significantly higher concentrations of PO_4^{3-}, NO_2^- and NO_3^- ($p < 0.01$). An average 6.4 ± 3.0 μM NO_3^- was found at this station, an order of magnitude higher than the other stations. SR3-5 station displayed a seawater-filled gap halfway through the ice cover, which could have supplied macronutrients to the ice.

3.4. Distribution of Chl*a* and POM

POC, PON, and PEPS showed different vertical distributions between fast and pack ice stations. L-shaped profiles characterized fast ice stations, while no clear vertical pattern was observed for pack ice (Figure 4). Although average Chl*a*, POC, PON, and PEPS did not statistically differ between pack and fast ice, higher bottom ice concentrations were found at the fast ice stations and higher surface-interior concentrations in pack ice stations ($p < 0.05$ for each parameter). Overall, PON and PEPS profiles matched the POC distribution for most stations. POC concentrations ranged from 4.1 μM in the ice surface layer of Mertz 3 to 260 μM at the lowermost section of Totten 1 (average 73.3 ± 27.6 μM for all stations). Particulate EPS concentrations in sea ice varied by three orders of magnitude, from 113 μg xeq. L^{-1} at the ice surface layer of Totten 2 to 16,290 μg xeq L^{-1} at the bottom of Totten 1. Average underice seawater POC and PEPS across all stations were 20.6 ± 12.5 μM and 454 ± 223 μg xeq L^{-1}, respectively (Table 2).
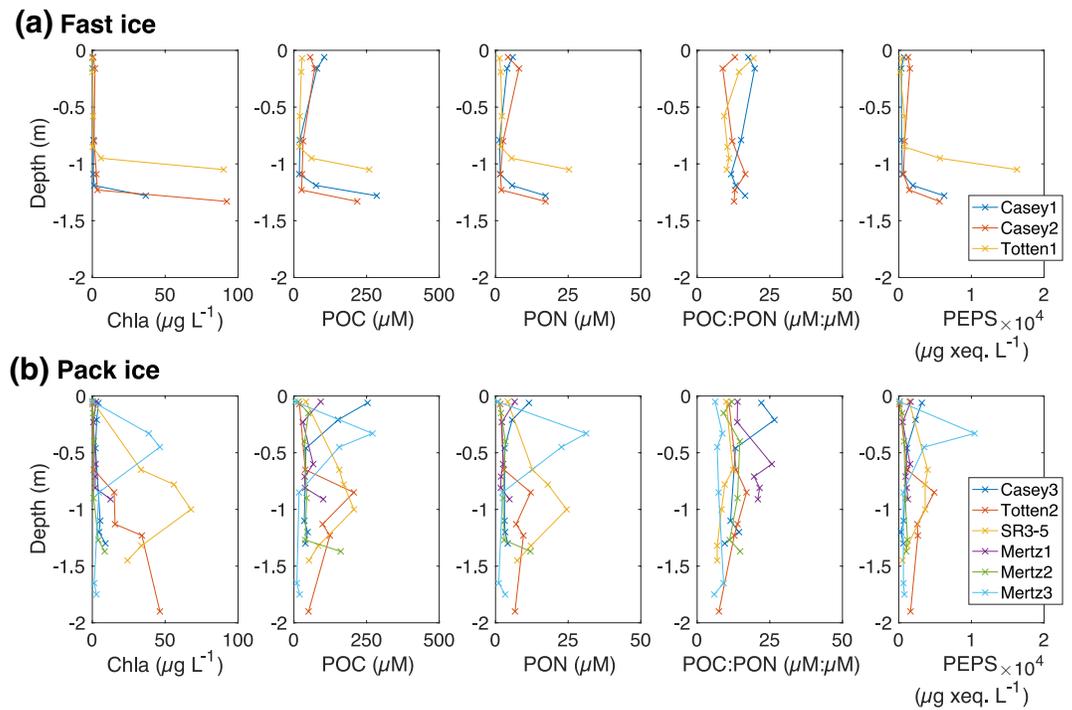
Figure 4. Vertical profiles of Chl*a*, POC, PON, POC:PON, and PEPS for fast (a) and pack (b) ice stations. Chl*a*, chlorophyll-*a*; POC, particulate organic carbon; PON, particulate organic nitrogen; PEPS, particulate exopolysaccharides.

3.5. Correlations Between Variables

Correlations between measured parameters were tested for fast and pack ice stations separately, and for all stations together (Figure 5). Results highlight a strong and significant correlation between PFe and PAl for
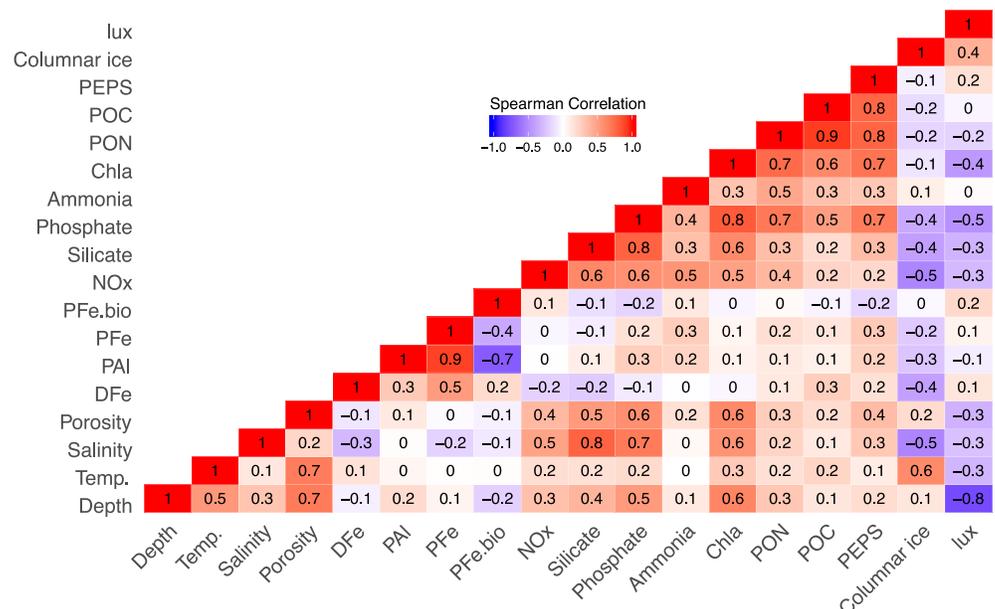

Figure 5. Spearman correlation matrix with all measured parameters for all (fast and pack ice) stations. Asterisks mark significant correlations at 95% confidence level ($p < 0.05$).

both pack (0.8; $p < 0.01$) and fast ice (0.9; $p < 0.01$). PEPS was correlated with POC, PON, and Chl$a$ ($\rho > 0.7$; $p < 0.01$) in fast, pack, and both ice types. There is also evidence of a moderate correlation of PEPS with salinity, ice porosity (0.5; 0.6; $p < 0.05$), macronutrients (0.5–0.8; $p < 0.05$) and NH_4^+ (0.5; $p < 0.01$) in fast ice, while PEPS was moderately correlated with PFe (0.5; $p < 0.01$) in pack ice. Chlorophyll a, POC, and PON were all related to one or more types of macronutrient at different degrees (0.4–0.8; $p < 0.05$) in fast ice. When all stations were analyzed together, salinity was moderately to strongly correlated (0.5–0.8; $p < 0.05$) with macronutrients but not with (dissolved and particulate) Fe. Finally, there is also a tendency of inverse correlation (not significant) of columnar ice with salinity, macro-nutrients and Fe for all ice stations.

4. Discussion

4.1. Summer Sea Ice Supports Heterotrophic Activity

Biomass and detritus are physically incorporated into newly forming sea ice and often show a uniform distribution over the ice thickness (Meiners et al., 2012; Thomas & Dieckmann, 2010). Throughout spring and summer though, other processes, for example, in-situ production and grazing, start shaping the vertical distribution of biomass. The relatively higher POC concentrations (both in fast and pack stations) observed in the top and intermediate ice layers compared to other seasons (Becquevort et al., 2009; Duprat et al., 2019; Janssens et al., 2016; Meiners et al., 2011; van der Merwe et al., 2011) suggest the upper ice cover becomes a more suitable habitat for sea-ice algae as the brine network connectivity increases during spring and summer. Heterotrophic processes are favored by the abundant presence of algal cell detritus and, potentially, EPS build up within these layers (Meiners, 2004, 2008). In the lowermost sections of the ice, we found C:N ratios (~12) deviating from the Redfield ratio of 6.6 for phytoplankton (Redfield et al., 1963) and approaching those usually associated with the presence of anaerobic micro-organisms in the rest of the ice (Rysgaard & Glud, 2004). A shift from an autotrophic bottom ice in spring toward a hetero-, and mixotrophic dominant environment could be driven by a potential decline in primary productivity associated with reduced nutrient availability and/or increased internal self-shading by ice algae. A higher C:N ratio could also indicate a relative increase of carbon associated with PEPS, which is known to be highly enriched in carbon relative to nitrogen (26 mol:mol; Engel & Passow, 2001).

Sea-ice concentrations of PEPS obtained here were consistently higher (average 946 μg xeq L^{-1}; 113–16,290 μg xeq L^{-1}) than those reported by van de Merwe et al. (2009) in East Antarctic spring sea ice (average 493 μg xeq L^{-1}; 2.84–2,690 μg xeq L^{-1}) indicating an ongoing microbial productivity from spring through summer. PEPS production could have also been intensified as a response to nutrient stress or changes in temperature and salinity conditions (Ewert & Deming, 2013). The relationship between PEPS and Chl$a$ ($\rho = 0.7$; $p < 0.01$) suggests autotrophic protists are involved in PEPS production. To date, it is still unknown to what extent sea-ice bacteria hydrolyze and degrade PEPS as a source of nutrition. Nevertheless, observations of sea-ice EPS-particles colonized by bacteria indicate this substrate is available for bacterial degradation (Meiners et al., 2004, 2008; Underwood et al., 2010). Therefore, PEPS could be used as a carbon source for bacteria, also facilitating grazing by heterotrophic and mixotrophic protists. Tightly coupled bacteria-algae interactions have been reported in sea-ice systems (Stewart & Fritsen, 2004) and the microbial loop is considered an important mechanism for recycling of organic matter in sea ice (Martin et al., 2012; Meiners and Michel, 2016).

4.2. Nitrate rather than Fe Limits Primary Production in Late Summer Sea Ice

Results from previous modeling (Saenz & Arrigo, 2014) and field studies (Lim et al., 2019; McMinn et al., 2000; Petrou et al., 2010) suggest that nutrients rather than light limit Antarctic sea-ice algae growth for the vast majority of the sunlit season. Sea-ice algae are also adapted to survive in a broad range of salinities, with particular tolerance to the low summer-ice salinity levels (Arrigo et al., 1993; Bates & Cota, 1986; Kirst & Wiencke, 1995; Palmisano et al. 1987; Ralph et al., 2007; Ryan et al., 2004; Torstensson et al., 2018). Based on these findings, macro- or micronutrients rather than light or salinity controlled autotrophic activity during our summer study.

Iron is considered the most limiting nutrient for phytoplankton growth in HNLC waters (Sunda, 2012). Sea-ice DFe levels in our study (~3 nM) were above the limitation threshold (~0.2 nM) for SO phytoplankton growth (Timmermans et al., 2004). We use Fe* to evaluate the potential Fe deficiency relative to PO_4^{3-} at this time of year. Scavenging of Fe commonly results in the decoupling of these elements (lower Fe relative to PO_4^{3-}) in most of the ocean surface waters (Parekh et al., 2005), especially in the SO where input from aeolian deposition is low (Gao et al., 2001). In our study, Fe* was always positive, indicating DFe was present in sufficient concentrations for complete utilization of the available PO_4^{3-}. It is worth considering that Fe:PO_4^{3-} was estimated based on oceanic phytoplankton ratios and that it is plausible that sea-ice diatoms could have evolved to less efficiently use Fe compared to pelagic assemblages, due to the abundance of this nutrient in sea ice relative to seawater (Lim et al., 2019). However, a Fe:PO_4^{3-} uptake ratio an order of magnitude higher would be necessary to observe some degree of Fe depletion relative to PO_4^{3-} in summer sea ice. A positive Fe* is also observed for the majority of the sea-ice samples if Fe* is calculated based on Fe to total DIN (dissolved inorganic nitrogen) uptake ratios for oceanic diatoms under both Fe limited and replete conditions (0.1–2.1 mmol:mol; Price, 2005). Our positive Fe* values suggest organic ligands should be present in sea ice in excess relative to DFe concentrations, therefore preventing Fe precipitation. Fe does not seem to limit primary production in summer sea ice, although we cannot rule out a potential co-limitation imposed by other essential micronutrients such as manganese and cobalt (Corami et al., 2005; Koch & Trimborn, 2019; Pausch et al., 2019; Schoffman et al., 2016).

A concomitant drawdown of PO_4^{3-} and $Si(OH)_4$ following the Redfield-Brzezinski nutrient ratio (Figure 3c; Brzezinski, 1985) was observed for most data points. This suggests a large contribution of diatoms to sea-ice primary production. Median (and interquartile) salinity normalized PO_4^{3-} (2.0 μM (4.3 μM)) and $Si(OH)_4$ (16.1 μM (24.1 μM)) concentrations show that the studied sea ice was enriched and partially depleted respectively compared to seawater (0.9 μM (0.6 μM) and 44.5 μM (34.3 μM)) at this time of the year. However, following the "Liebig's Law" (von Liebig, 1940) which states that growth should be limited by the most deficient nutrient, the fact that PO_4^{3-} is above the Redfield N:P ratio (16; Figure 3b) indicates that DIN is the primary limiting nutrient in summer sea ice. Nitrate:PO_4^{3-} depletion was previously observed under Fe replete conditions during mesoscale Fe-enrichment experiments in HNLC waters (Boyd et al., 2000). In the present study, bulk nitrate and nitrite (NO_x) concentrations are close to exhaustion (<0.2 μM) at Casey 1, Totten 2, Mertz 1, 2, and 3. Brine concentrations < 0.2 μM were also observed at Mertz 2 and Mertz 3. In the absence of other sources of nitrogen NH_4^+ would be readily consumed shortly after production. This could explain why our bulk NH_4^+ concentrations are amongst the lowest ever reported in Antarctic sea ice (Fripiat et al., 2017). The low concentrations of N-sources found in most ice floes could therefore impose severe limitations for sympagic algal growth. Enhanced ice melting during summer exacerbates stratification within the ice, preventing convection-driven brine exchanges and replenishment of nutrients from seawater. This scenario would render sea ice particularly dependent on recycling and/or seawater intrusion to alleviate macronutrient limitation at this time of the year.

4.3. Sea-Ice PFe as a Capacitor for Summer Blooms

Warmer air temperatures lead to increased connectivity of the brine network forming new pathways for brine, meltwater and associated nutrient drainage toward the seawater underneath. As a consequence, DFe concentrations in sea ice collected at this time of the year are expected to be low. However, the sea-ice DFe concentrations up to 13.3 nM (Figure 3a) were comparable to those reported from other seasons (Lannuzel, et al., 2016, and references therein). DFe is therefore likely continuously supplied to sea ice either as truly soluble Fe or in the colloidal form, despite brine drainage and ice decay. Many studies have shown the importance of the PFe in replenishing the DFe pool via thermal, photochemical, biological and ligand-mediated dissolution (Borer et al., 2005; Ellwood et al., 2012; Kraemer, 2004; Sulzberger et al., 1989). These biogeochemical processes could have potentially maintained background levels of DFe (average 4.7 ± 3.8 nM and 2.0 ± 1.3 nM for fast and pack ice, respectively) at our sea ice stations. Particulate Fe is retained within sea ice longer than DFe because of the adsorption of particles to the walls of the brine channels, a process possibly facilitated by EPS (Becquevort et al., 2009; Lannuzel et al., 2016; van der Merwe et al., 2011). EPS are particularly abundant in waters characterized by high chlorophyll concentrations and in the sea ice

(Gledhill & Buck, 2012). Although they are predominantly composed of neutral sugars, EPS contain a significant fraction of uronic acids which are known to complex Fe (Mancuso Nichols et al., 2004).

Relatively high concentrations of calculated PFe_{bio} (∼50 nM) were observed for all pack ice stations over the entire ice thickness. Since Al is not appreciably accumulated into biogenic material, this result indicates the occurrence of biological assimilation and build-up of biogenic PFe at all ice depths. Based on the measurements of Fe concentration and sea-ice thickness from the sampled cores, if all of the sea ice represented by our samples melts by the end of austral summer (∼60 days between the sampling period and the end of February), an average of 4.6 ± 7.1 $\mu mol\ m^{-2}\ d^{-1}$ PFe would be released from sea ice into East-Antarctic surface waters. This input could be particularly important during this time of the year due to the stronger ocean stratification driven by sea-ice melt and ocean surface warming, which hamper the mixing with Fe-rich deep waters. Pack ice formed in coastal polynyas is exposed to coastal Fe inputs and could therefore play a crucial role in delivering biologically processed (and potentially bioavailable) PFe to open waters. In this context, the contribution of summer sea ice as a source of (both biogenic and lithogenic) PFe cannot be neglected. The direct link between PFe solubility and phytoplankton growth however needs to be established, as well as the possible forward trajectories of ice floes into Fe-limited waters, before we will be able to adequately assess the effect of sea ice on the carbon cycle.

4.4. Can Sea Ice Enhance the Fertilization Potential From Glacial Fe?

Iron distribution in East Antarctic sea ice did not show significant spatial variation in this study, except for Totten 1, with DFe and PFe concentrations significantly higher than those found elsewhere (average 7.0 and 1,800 nM, respectively). The level of PFe measured in bottom sea ice at Totten 1 (∼5 μM) was only comparable to concentrations found in bottom sea ice collected in the Ross Sea (Grotti et al., 2001; Noble et al., 2013) and at a study site of very shallow (∼20 m depth) bathymetry near Casey station (van der Merwe et al., 2011). The average molar PFe:PAl (0.3 ± 0.1) obtained from Totten 1 ice is very close to values previously reported for the continental crust (0.3; Taylor & McLennan, 1985), suggesting a predominantly lithogenic source. Interestingly, this elemental ratio differs significantly ($p < 0.01$) from the ones measured at Casey 1 and 2 (0.5 ± 0.2), which were very close to the ratio reported for ocean floor sediments (0.48; Ravanelli, 1997). Therefore, while stations near Casey seem to be highly dependent on sediment resuspension as the main source of Fe, another source may prevail at Totten 1. The low PFe content in the snow at Totten 1 indicates atmospheric sources are unlikely. Iron must instead come from below, either by vertical or lateral transport. The most substantial geographical features in the proximity of Totten 1 are the Totten Ice Shelf and the Moscow University Ice Shelf (MUIS). We therefore hypothesize the presence of basal meltwater from the adjacent MUIS and potentially meltwater runoff from the dominant Totten Ice Shelf could explain the high Fe content observed at this station.

Seawater Fe levels have been previously reported to be significantly influenced by glacial melting around Antarctica (Death et al., 2014; Herraiz-Borreguero et al., 2016; I. Kim et al., 2015; Person et al., 2019). This effect is attributed to the fact that glacial meltwater can supply intensively physically and chemically weathered Fe-rich labile sediments (Raiswell et al., 2018 and references therein; van der Merwe et al., 2019). Glaciogenic minerals are also enriched in labile Fe^{2+} nanoparticulates compared to other lithogenic sources which are mostly comprised of less bioavailable Fe^{3+} oxyhydroxide and other Fe^{3+} chemical-weathered oxide products (Hawkings et al., 2018; Shoenfelt et al., 2017). While some of this glacial material can be incorporated into marine ice along with upwelling transport, a fraction can also be carried within the ice shelf meltwater plume and reach surface waters (Herraiz-Borreguero et al., 2016). Layers of granular and platelet ice were evident at Totten 1. Supercooled glacial meltwaters from the nearby MUIS could promote the formation of these ice structures. The abundant particles contained in these meltwaters could act as crystallization nuclei and therefore facilitate the formation of frazil ice. These crystals can then rise through the water column scavenging Fe-rich suspended sediments in shallow waters near the coast or at the grounding line of ice shelves to be incorporated into the sea ice, analogous to marine ice under an ice shelf (de Jong et al., 2013; Herraiz-Borreguero et al., 2016). The high proportion of platelet ice within the noncolumnar ice at Totten 1 strengthens the link between Fe-rich glacial meltwater and the high concentration of PFe found at the bottom of Totten 1.
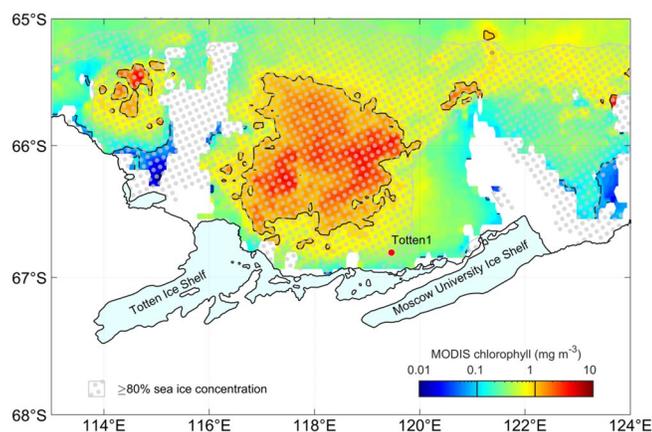
Figure 6. Above: Moderate Resolution Imaging Spectroradiometer (MODIS)-Aqua summer chlorophyll-a concentrations (December—February climatology) off the Sabrina Coast from 2002 to 2016, also indicating the location of Totten 1 station. White regions indicate areas where no data is available due to grounded iceberg and fast ice coverage.

Within the sea ice, Fe can be converted into more readily available forms via abiotic (photoreduction and chemical complexation) and biotic (biological and enzymatic reduction at the cell surface) processes (Genovese et al., 2018; Kaplan & Ward, 2013; Tagliabue et al., 2009). Fe dissolution reactions could be augmented by freezing processes. Repetitive freeze/thaw cycles have been shown to continuously add DFe to the ice. Freezing concentrates water and solutes into microenvironments at grain boundaries (Jeong et al., 2020, 2012; K. Kim et al., 2010). However, Fe^{3+} addition to an enclosed system is limited by saturation, therefore Fe^{3+} is prone to incorporation into the colloidal phase or adsorption onto ice crystals (Raiswell et al., 2018). When sea ice melts, the undersaturated meltwater can stimulate further Fe dissolution to occur. Layers of superimposed ice found in our ice-core samples suggest that melting and refreezing is common in summer sea ice in this area. Therefore, the interaction between glacially derived reactive sediments and sea ice could enhance productivity by releasing elevated concentrations of highly recycled and potentially bioavailable Fe during the melting season, when this stock becomes exhausted in surface waters (Sedwick et al., 2000). Additional offshore transport of sea ice formed in coastal areas could further enhance the extent of Fe fertilization.

Findings from Totten 1 raise the question why similar Fe enrichment in sea ice was not observed at the other stations near ice shelves that we sampled along the East Antarctic coast. Mertz 2 station was relatively close (∼1 km) to the Mertz glacier. Results from past oceanographic surveys could explain this difference. Waters on the continental shelf in East Antarctica are relatively cool, leading to low rates of basal melt from the ice shelves. The Totten and MUIS are exceptions to this general pattern as relatively warm modified Circumpolar Deep Water (mCDW) enters the cavity beneath the shelf through a deep trough, delivering sufficient heat to drive rapid basal melt (Rintoul et al., 2016). Silvano et al. (2017) showed that this mCDW is widespread over the continental shelf of the Sabrina Coast. Based on this oceanographic particularity, the Totten/MUIS glacial basin could offer the required hydrographic setting for the recurrent formation of Fe-rich platelet ice to potentially occur in large areas of the Sabrina Coast. While Fe supplied from these glaciers is not essential for the sea-ice communities, it might play an important role for phytoplankton communities when this sea ice melts along the Sabrina Coast.

Satellite Chl*a* imagery from 2002 to 2016 supports the link between the presence of platelet ice and surface water fertilization in the surroundings of Totten 1 (Figure 6). The summer climatology suggests that large phytoplankton biomass accumulates when the sea ice in front of the Totten Glacier breaks out. This contrasts with the rather low productivity of the neighboring Dalton Polynya that is in front of the MUIS (Moreau et al., 2019). The outflow of glacial meltwater from the Totten Ice Shelf is located on the western side of the calving front (Silvano et al., 2018). The outflow of glacial meltwater from the MUIS is widespread along the coast and south of the Dalton polynya, with productivity highest in the latter region (Moreau et al., 2019). To our knowledge, these observations could be the first evidence of a potential fertilization impact from the combined presence of platelet ice and Fe-rich glacial meltwaters. The Totten glacier mass loss has increased through time from 5.7 Gt y^{-1} in 1979–2003 to 7.3 Gt y^{-1} in 2003–2017; glaciers draining into MUIS show a slight net thinning in the last decades (Rignot et al., 2019). As climate change could drive the loss of up to 23% of the ice shelf volume in Antarctica by 2070 in a business-as-usual scenario (DeConto & Pollard, 2016; Rintoul et al., 2018), a better understanding of how marine and glacial sediment transport will be affected by increasing basal melting and grounding line retreat is needed.

5. Conclusion

The scarcity of inorganic nitrogen sources along with abundant particulate matter suggest the dominance of heterotrophic and potentially mixotrophic activity in sea ice during summer. At this time of the year, the sea ice can still retain a significant amount of Fe, both in the dissolved and, particularly, in the particulate

fraction. Biotic and abiotic processes help sustain Fe supply during late summer. Projected changes in sea-ice thickness and snowfall could increase fluxes of macronutrients via surface flooding and brine percolation, alleviating nutrient depletion in summer, and potentially extending the period of habitability for sea-ice algae. Climate change might also impose indirect impacts on the sea-ice Fe distribution via reduction of glacial coverage in Antarctica. In East Antarctica, the Totten Ice Shelf is already experiencing rapid basal melt. A further increase in the supply of glacial meltwater to the East Antarctic shelf could potentially stimulate the formation of platelet ice layers in the surrounding sea ice. How phytoplankton will be affected by this reservoir of Fe will depend both on the timing of its release to surface waters and on the bioavailability of this source which is a function of the biological and physicochemical changes that Fe undergoes within the ice.

Data Availability Statement

Data supporting the analysis and conclusions here presented can be accessed through the Australian Antarctic Data Centre website (https://data.aad.gov.au/metadata/records/AAV2_seaice_BGC_2016).

References

Allison, I. (1998). The East Antarctic sea ice zone: Ice characteristics and drift. *GeoJournal*, *18*, 103–115.

Arar, E. J., & Collins, G. B. (1997). *Method 445.0 in vitro determination of chlorophyll-a and pheophytin-a in marine and freshwater algae by fluorescence*. Washington, DC.U.S. Environmental Protection Agency.

Arndt, S., Meiners, K. M., Ricker, R., Krumpen, T., Katlein, C., & Nicolaus, M. (2017). Influence of snow depth and surface flooding on light transmission through Antarctic pack ice. *Journal of Geophysical Research: Oceans*, *122*(3), 2108–2119. https://doi.org/10.1002/2016jc012325

Arrigo, K. R., Kremer, J. N., & Sullivan, C. W. (1993). A simulated Antarctic fast ice ecosystem. *Journal of Geophysical Research*, *98*(C4), 6929–6946. https://doi.org/10.1029/93jc00141

Arrigo, K. R., Mills, M. M., Kropuenske, L. R., van Dijken, G. L., Alderkamp, A. C., & Robinson, D. H. (2010). Photophysiology in two major Southern-Ocean phytoplankton taxa: Photosynthesis and growth of *Phaeocystis antarctica* and *Fragilariopsis cylindrus* under different irradiance levels. *Integrative and Comparative Biology*, *50*(6), 950–966. https://doi.org/10.1093/icb/icq021

Arrigo, K. R., Perovich, D. K., Pickart, R. S., Brown, Z. W., van Dijken, G. L., Lowry, K. E., et al. (2012). Massive phytoplankton blooms under Arctic sea ice. *Science*, *336*(6087), 1408. https://doi.org/10.1126/science.1215065

Arrigo, K. R., Weiss, A. M., & Smith, W. O. (1998). Physical forcing of phytoplankton dynamics in the southwestern Ross Sea. *Journal of Geophysical Research*, *103*(C1), 1007–1021. https://doi.org/10.1029/97jc02326

Azam, K., & Singh, K. N. (2013). Evaluation of relationship between light intensity (lux) and growth of *Chaetoceros muelleri*. *Oceanography: Open Access*, *1*(3). https://doi.org/10.4172/2332-2632.1000111

Baar, H. J. W. D., Burna, A. G., Nolting, R. F., Cadee, G. C., Jacques, G., & Treguer, P. (1990). On iron limitation of the Southern Ocean: Experimental observations in the Weddell and Scotia seas. *Marine Ecology Progress Series*, *65*, 105–122. https://doi.org/10.3354/meps065105

Baar, H. J. W. D., Dejong, J. T. M., Bakker, D. C. E., Loscher, B. M., Veth, C., Bathmann, U., & Smetacek, V. (1995). Importance of iron for plankton blooms and carbon-dioxide drawdown in the Southern Ocean. *Nature*, *373*(6513), 412–415. https://doi.org/10.1038/373412a0

Bates, S. S., & Cota, G. F. (1986). Fluorescence induction and photosynthetic responses of Arctic ice algae to sample treatment and salinity. *Journal of Phycology*, *22*(4), 421–429. https://doi.org/10.1111/j.1529-8817.1986.tb02484.x

Becquevort, S., Dumont, I., Tison, J. L., Lannuzel, D., Sauvée, M. L., Chou, L., & Schoemann, V. (2009). Biogeochemistry and microbial community composition in sea ice and underlying seawater off East Antarctica during early spring. *Polar Biology*, *32*(6), 879–895. https://doi.org/10.1007/s00300-009-0589-2

Bertrand, E. M., Saito, M. A., Lee, P. A., Dunbar, R. B., Sedwick, P. N., & Ditullio, G. R. (2011). Iron limitation of a springtime bacterial and phytoplankton community in the Ross Sea: Implications for vitamin B(12) nutrition. *Frontiers in Microbiology*, *2*, 160. https://doi.org/10.3389/fmicb.2011.00160

Bombosch, A. (2013). Interactions between floating ice platelets and ocean water in the southern Weddell sea. In S. S. Jacobs, & R. F. Weiss (Eds.), Ocean, ice, and atmosphere: Interactions at the Antarctic continental margin (Vol. 75, pp. 257–266). Washington, DC: American Geophysical Union. https://doi.org/10.1029/AR075p0257

Borer, P. M., Sulzberger, B., Reichard, P., & Kraemer, S. M. (2005). Effect of siderophores on the light-induced dissolution of colloidal iron(III) (hydr)oxides. *Marine Chemistry*, *93*(2–4), 179–193. https://doi.org/10.1016/j.marchem.2004.08.006

Bowie, A. R., Townsend, A. T., Lannuzel, D., Remenyi, T. A., & van der Merwe, P. (2010). Modern sampling and analytical methods for the determination of trace elements in marine particulate material using magnetic sector inductively coupled plasma-mass spectrometry. *Analytica Chimica Acta*, *676*(1–2), 15–27. https://doi.org/10.1016/j.aca.2010.07.037

Boyd, P. W., Watson, A. J., Law, C. S., Abraham, E. R., Trull, T., Murdoch, R., et al. (2000). A mesoscale phytoplankton bloom in the polar Southern Ocean stimulated by iron fertilization. *Nature*, *407*(6805), 695–702. https://doi.org/10.1038/35037500

Brandt, R. E., Warren, S. G., Worby, A. P., & Grenfell, T. C. (2005). Surface albedo of the Antarctic sea ice zone. *Journal of Climate*, *18*(17), 3606–3622. https://doi.org/10.1175/jcli3489.1

Brzezinski, M. A. (1985). The Si:C:N ratio of marine diatoms: Interspecific variability and the effect of some environmental variables. *Journal of Phycology*, *21*(3), 347–357. https://doi.org/10.1111/j.0022-3646.1985.00347.x

Corami, F., Capodaglio, G., Turetta, C., Soggia, F., Magi, E., & Grotti, M. (2005). Summer distribution of trace metals in the western sector of the Ross Sea, Antarctica. *Journal of Environmental Monitoring*, *7*(12), 1256–1264. https://doi.org/10.1039/b507323p

de Jong, J., Schoemann, V., Lannuzel, D., Croot, P., de Baar, H., & Tison, J.-L. (2012). Natural iron fertilization of the Atlantic sector of the Southern Ocean by continental shelf sources of the Antarctic Peninsula. *Journal of Geophysical Research*, *117*(G1). https://doi.org/10.1029/2011jg001679

de Jong, A., Schoemann, V., Maricq, N., Mattielli, N., Patricia, L.H. T., & Tison, J. L. (2013). Iron in land-fast sea ice of McMurdo Sound derived from sediment resuspension and wind-blown dust attributes to primary productivity in the Ross Sea, Antarctica. *Marine Chemistry*, *157*, 24–40. https://doi.org/10.1016/j.marchem.2013.07.001

Death, R., Wadham, J. L., Monteiro, F., Le Brocq, A. M., Tranter, M., Ridgwell, A.&, et al. (2014). Antarctic ice sheet fertilises the Southern Ocean. *Biogeosciences*, *11*(10), 2635–2643. https://doi.org/10.5194/bg-11-2635-2014

DeConto, R. M., & Pollard, D. (2016). Contribution of Antarctica to past and future sea-level rise. *Nature*, *531*(7596), 591–597. https://doi.org/10.1038/nature17145

Duprat, L., Kanna, N., Janssens, J., Roukaerts, A., Deman, F., Townsend, A. T., et al. (2019). Enhanced iron flux to Antarctic sea ice via dust deposition from ice-free coastal areas. *Journal of Geophysical Research: Oceans*. https://doi.org/10.1029/2019jc015221*124*(12), 8538–8557.

Ellwood, M. J., Hutchins, D. A., Lohan, M. C., Milne, A., Nasemann, P., Nodder, S. D., et al. (2015). Iron stable isotopes track pelagic iron cycling during a subtropical phytoplankton bloom. *Proceedings of the Natinal Academic of Science U S A*, *112*, E15–E20. https://doi.org/10.1073/pnas.1421576112

Engel, A., & Passow, U. (2001). Carbon and nitrogen content of transparent exopolymer particles (TEP) in relation to their Alcian blue adsorption. *Marine Ecology Progress Series*, *219*, 1–10. https://doi.org/10.3354/meps219001

Ewert, M., & Deming, J. W. (2013). sea ice microorganisms: Environmental constraints and extracellular responses. *Biology*, *2*, 603–628. https://doi.org/10.3390/biology2020603

Fripiat, F., Meiners, K. M., Vancoppenolle, M., Papadimitriou, S., Thomas, D. N., Ackley, S. F., et al. (2017). Macro-nutrient concentrations in Antarctic pack ice: Overall patterns and overlooked processes. *Elementa-Science of the Anthropocene*, *5*. https://doi.org/10.1525/elementa.217*(13), 2–24.

Gao, Y., Kaufman, Y. J., Tanre, D., Kolber, D., & Falkowski, P. G. (2001). Seasonal distributions of aeolian iron fluxes to the global ocean. *Geophysical Research Letters*, *28*(1), 29–32. https://doi.org/10.1029/2000gl011926

Genovese, C., Grotti, M., Pittaluga, J., Ardini, F., Janssens, J., Wuttig, K., et al. (2018). Influence of organic complexation on dissolved iron distribution in East Antarctic pack ice. *Marine Chemistry*, *203*, 28–37. https://doi.org/10.1016/j.marchem.2018.04.005

Gledhill, M., & Buck, K. N. (2012). The organic complexation of iron in the marine environment: A review. *Frontiers in Microbiology*, *3*, 69. https://doi.org/10.3389/fmicb.2012.00069

Gradinger, R., & Ikavalko, J. (1998). Organism incorporation into newly forming Arctic sea ice in the Greenland Sea. *Journal of Plankton Research*, *20*(5), 871–886. https://doi.org/10.1093/plankt/20.5.871

Grotti, M., Soggia, F., Abelmoschi, M. L., Rivaro, P., Magi, E., & Frache, R. (2001). Temporal distribution of trace metals in Antarctic coastal waters. *Marine Chemistry*, *76*(3), 189–209. https://doi.org/10.1016/S0304-4203(01)00063-9

Haas, C., Thomas, D. N., & Bareiss, J. (2017). Surface properties and processes of perennial Antarctic sea ice in summer. *Journal of Glaciology*, *47*(159), 613–625. https://doi.org/10.3189/172756501781831864

Hancke, K., Lund-Hansen, L. C., Lamare, M. L., Højlund Pedersen, S., King, M. D., Andersen, P., & Sorrell, B. K. (2018). Extreme low light requirement for algae growth underneath sea ice: A case study from station Nord, NE Greenland. *Journal of Geophysical Research: Oceans*, *123*(2), 985–1000. https://doi.org/10.1002/2017jc013263

Hawkings, J. R., Benning, L. G., Raiswell, R., Kaulich, B., Araki, T., Abyaneh, M., et al. (2018). Biolabile ferrous iron bearing nanoparticles in glacial sediments. *Earth and Planetary Science Letters*, *493*, 92–101. https://doi.org/10.1016/j.epsl.2018.04.022

Herraiz-Borreguero, L., Lannuzel, D., van der Merwe, P., Treverrow, A., & Pedro, J. B. (2016). Large flux of iron from the Amery ice shelf marine ice to Prydz Bay, East Antarctica. *Journal of Geophysical Research: Oceans*, *121*(8), 6009–6020. https://doi.org/10.1002/2016jc011687

Janssens, J., Meiners, K. M., Tison, J. L., Dieckmann, G., Delille, B., & Lannuzel, D. (2016). Incorporation of iron and organic matter into young Antarctic sea ice during its initial growth stages. *Elementa-Science of the Anthropocene*, *4*, 000123. https://doi.org/10.12952/journal.elementa.000123

Jeong, D., Kim, K., & Choi, W. (2012). Accelerated dissolution of iron oxides in ice. *Atmospheric Chemistry and Physics*, *12*, 11125–11133. https://doi.org/10.5194/acp-12-11125-2012

Jeong, D., Kim, K., Min, D. W., & Choi, W. (2020). Freezing-enhanced dissolution of iron oxides: Effects of inorganic acid Anions. *Environmental Science Technology*, *49*, 12816–12822. https://doi.org/10.1021/acs.est.5b04211

Kaplan, J., & Ward, D. M. (2013). The essential nature of iron usage and regulation. *Current Biology*, *23*(15), R642–R646. https://doi.org/10.1016/j.cub.2013.05.033

Katlein, C., Arndt, S., Nicolaus, M., Perovich, D. K., Jakuba, M. V., Suman, S., et al. (2015). Influence of ice thickness and surface properties on light transmission through Arctic sea ice. *Journal of Geophysical Research: Oceans*, *120*(9), 5932–5944. https://doi.org/10.1002/2015JC010914

Kérouel, R., & Aminot, A. (1997). Fluorometric determination of ammonia in sea and estuarine waters by direct segmented flow analysis. *Marine Chemistry*, *57*(3–4), 265–275. https://doi.org/10.1016/s0304-4203(97)00040-6

Kim, K., Choi, W., Hoffmann, M. R., Yoon, H. I., & Park, B. K. (2010). Photoreductive dissolution of iron oxides trapped in ice and its environmental implications. *Environmental Science & Technolology*, *44*(11), 4142–4148. https://doi.org/10.1021/es9037808

Kim, I., Kim, G., & Choy, E. J. (2015). The significant inputs of trace elements and rare earth elements from melting glaciers in Antarctic coastal waters. *Polar Research*, *34*(1). https://doi.org/10.3402/polar.v34.2428924289

Kirst, G. O., & Wiencke, C. (1995). Ecophysiology of polar algae. *Journal of Phycology*, *31*(2), 181–199. https://doi.org/10.1111/j.0022-3646.1995.00181.x

Koch, F., & Trimborn, S. (2019). Limitation by Fe, Zn, Co, and B12 results in similar physiological responses in two Antarctic phytoplankton species. *Frontiers in Marine Science*, *6*. https://doi.org/10.3389/fmars.2019.00514(514),

Kraemer, S. M. (2004). Iron oxide dissolution and solubility in the presence of siderophores. *Aquatic Sciences: Research Across Boundaries*, *66*(1), 3–18. https://doi.org/10.1007/s00027-003-0690-5

Lancelot, C., de Montety, A., Goosse, H., Becquevort, S., Schoemann, V., Pasquer, B., & Vancoppenolle, M. (2009). Spatial distribution of the iron supply to phytoplankton in the Southern Ocean: A model study. *Biogeosciences*, *6*(12), 2861–2878. https://doi.org/10.5194/bg-6-2861-2009

Langhorne, P. J., Hughes, K. G., Gough, A. J., Smith, I. J., Williams, M. J. M., Robinson, N. J., et al. (2015). Observed platelet ice distributions in Antarctic sea ice: An index for ocean-ice shelf heat flux. *Geophysical Research Letters*, *42*(13), 5442–5451. https://doi.org/10.1002/2015gl064508

Langway, C. C., Jr. (1958). Ice fabrics and the universal stage. In *Snow, ice and permafrost research establishment* (Technical Report U.S. 62).

Lannuzel, D., Chever, F., van der Merwe, P. C., Janssens, J., Roukaerts, A., Cavagna, A. J., et al. (2016). Iron biogeochemistry in Antarctic pack ice during SIPEX-2. *Deep-Sea Research Part II-Topical Studies in Oceanography*, *131*, 111–122. https://doi.org/10.1016/j.dsr2.2014.12.003

Lannuzel, D., de Jong, J., Schoemann, V., Trevena, A., Tison, J. L., & Chou, L. (2006). Development of a sampling and flow injection analysis technique for iron determination in the sea ice environment. *Analytica Chimica Acta*, *556*(2), 476–483. https://doi.org/10.1016/j.aca.2005.09.059

Lannuzel, D., Schoemann, V., de Jong, J., Chou, L., Delille, B., Becquevort, S., & Tison, J. L. (2008). Iron study during a time series in the western Weddell pack ice. *Marine Chemistry*, *108*(1–2), 85–95. https://doi.org/10.1016/j.marchem.2007.10.006

Lannuzel, D., Schoemann, V., de Jong, J., Tison, J. L., & Chou, L. (2007). Distribution and biogeochemical behaviour of iron in the East Antarctic sea ice. *Marine Chemistry*, *106*(1–2), 18–32. https://doi.org/10.1016/j.marchem.2006.06.010

Lannuzel, D., Schoemann, V., Dumont, I., Content, M., de Jong, J., Tison, J. L., et al. (2013). Effect of melting Antarctic sea ice on the fate of microbial communities studied in microcosms. *Polar Biology*, *36*(10), 1483–1497. https://doi.org/10.1007/s00300-013-1368-7

Lannuzel, D., Vancoppenolle, M., van der Merwe, P., de Jong, J., Meiners, K. M., Grotti, M., et al. (2016). Iron in sea ice: Review and new insights. *Elementa: Science of the Anthropocene*, *4*, 000130. https://doi.org/10.12952/journal.elementa.000130

von Liebig, J. Y. (1940). L. Playfair *Organic chemistry in its applications to agriculture and physiology*, 1st ed., . Cambridge, UK. https://doi.org/10.5962/bhl.title.40751 John Owen.

Lim, S. M., Moreau, S., Vancoppenolle, M., Deman, F., Roukaerts, A., Meiners, K. M., et al. (2019). Field observations and physical-biogeochemical modeling suggest low silicon affinity for Antarctic fast-ice diatoms. *Journal of Geophysical Research: Oceans*. https://doi.org/10.1029/2018jc014458 *124*(11), 7837–7853.

Mancuso Nichols, C. A., Garon, S., Bowman, J. P., Raguenes, G., & Guezennec, J. (2004). Production of exopolysaccharides by Antarctic marine bacterial isolates. *Journal of Applied Microbiology*, *96*, 1057–1066. https://doi.org/10.1111/j.1365-2672.2004.02216.x

Markussen, T. N., Elberling, B., Winter, C., & Andersen, T. J. (2016). Flocculated meltwater particles control Arctic land-sea fluxes of labile iron. *Scientific Reports*, *6*, 24033. https://doi.org/10.1038/srep24033

Martin, J. H. (1990). Glacial-interglacial CO_2 change: The iron hypothesis. *Paleoceanography*, *5*(1), 1–13. https://doi.org/10.1029/PA005i001p00001

Martin, J. H. (1993). Determination of particulate organic carbon (POC) and nitrogen (PON) in seawater. In S. Kadar, M. Leinen, & J. W. Murray (Eds.), ,Equatorial Pacific process study sampling and—Analytical protocol(37–48). U. S. JGOFS.

Martin, A., McMinn, A., Davy, S. K., Anderson, M. J., Miller, H. C., Hall, J. A., & Ryan, K. G. (2012). Preliminary evidence for the microbial loop in Antarctic sea ice using microcosm simulations. *Antarctic Science*, *24*(6), 547–553. https://doi.org/10.1017/S0954102012000491

Massom, R. A., & Stammerjohn, S. E. (2010). Antarctic sea ice change and variability - physical and ecological implications. *Polar Science*, *4*(2), 149–186. https://doi.org/10.1016/j.polar.2010.05.001

McMinn, A., Ashworth, C., & Ryan, K. G. (2000). In situ net primary productivity of an Antarctic fast ice bottom algal community. *Aquatic Microbial Ecology*, *21*(2), 177–185. https://doi.org/10.3354/ame021177

Meiners, K. M., Brinkmeyer, R., Granskog, M. A., & Lindfors, A. (2004). Abundance, size distribution and bacterial colonization of exopolymer particles in Antarctic sea ice (Bellingshausen Sea). *Aquatic Microbial Ecology*, *35*(3), 283–296. https://doi.org/10.3354/ame035283

Meiners, K. M., Krembs, C., & Gradinger, R. (2008). Exopolymer particles: Microbial hotspots of enhanced bacterial activity in Arctic fast ice (Chukchi Sea). *Aquatic Microbial Ecology*, *52*(2), 195–207. https://doi.org/10.3354/ame01214

Meiners, K. M., & Michel, C. (2016). Dynamics of nutrients dissolved organic matter and exopolymers in sea ice. In D. N. Thomas (Ed.), *Sea ice*, 3rd Edition, (pp. 415–432). https://doi.org/10.1002/9781118778371.ch17 Oxford: Wiley-Blackwell.

Meiners, K. M., Norman, L., Granskog, M. A., Krell, A., Heil, P., & Thomas, D. N. (2011). Physico-ecobiogeochemistry of East Antarctic pack ice during the winter-spring transition. *Deep Sea Research Part II: Topical Studies in Oceanography*, *58*(9–10), 1172–1181. https://doi.org/10.1016/j.dsr2.2010.10.033

Meiners, K. M., Vancoppenolle, M., Thanassekos, S., Dieckmann, G. S., Thomas, D. N., Tison, J. L., et al. (2012). Chlorophylla in Antarctic sea ice from historical ice core data. *Geophysical Research Letters*, *39*(21). https://doi.org/10.1029/2012gl053478

Moreau, S., Lannuzel, D., Janssens, J., Arroyo, M. C., Corkill, M., Cougnon, E., et al. (2019). Sea ice meltwater and Circumpolar Deep-Water drive contrasting productivity in three Antarctic polynyas. *Journal of Geophysical Research: Oceans*, *124*(5), 2943–2968. https://doi.org/10.1029/2019jc015071

Morel, F. M. M., Kustka, A. B., & Shaked, Y. (2008). The role of unchelated Fe in the iron nutrition of phytoplankton. *Limnology and Oceanography*, *53*(1), 400–404. https://doi.org/10.4319/lo.2008.53.1.0400

Noble, A. E., Moran, D. M., Allen, A. E., & Saito, M. A. (2013). Dissolved and particulate trace metal micronutrients under the McMurdo Sound seasonal sea ice: Basal sea ice communities as a capacitor for iron. *Frontiers in Chemistry*, *1*(25), 25. https://doi.org/10.3389/fchem.2013.00025

Oerter, H., Kipfstuhl, J., Determann, J., Miller, H., Wagenbach, D., Minikin, A., & Graf, W. (1992). Evidence for basal marine ice in the Filchner-Ronne ice shelf. *Nature*, *358*(6385), 399–401. https://doi.org/10.1038/358399a0

Palmisano, A. C., Beeler SooHoo, J., & Sullivan, C. W. (1987). Effects of four environmental variables on photosynthesis-irradiance relationships in Antarctic sea-ice microalgae. *Marine Biology*, *94*(2), 299–306. https://doi.org/10.1007/bf00392944

Paolo, F. S., Fricker, H. A., & Padman, L. (2015). Ice sheets. Volume loss from Antarctic ice shelves is accelerating. *Science*, *348*(6232), 327–331. https://doi.org/10.1126/science.aaa0940

Parekh, P., Follows, M. J., & Boyle, E. A. (2005). Decoupling of iron and phosphate in the global ocean. *Global Biogeochemical Cycles*, *19*(2). https://doi.org/10.1029/2004gb002280

Passow, U., & Alldredge, A. L. (1994). Distribution, size and bacterial colonization of transparent exopolymer particles (TEP) in the ocean. *Marine Ecology Progress Series*, *113*(1–2), 185–198. https://doi.org/10.3354/meps113185

Pausch, F., Bischof, K., & Trimborn, S. (2019). Iron and manganese co-limit growth of the Southern Ocean diatom Chaetoceros debilis. *PLoS One*, *14*(9), e0221959. https://doi.org/10.3354/meps113185

Person, R., Aumont, O., Madec, G., Vancoppenolle, M., Bopp, L., & Merino, N. (2019). Sensitivity of ocean biogeochemistry to the iron supply from the Antarctic Ice Sheet explored with a biogeochemical model. *Biogeosciences*, *16*(18), 3583–3603. https://doi.org/10.5194/bg-16-3583-2019

Petrou, K., Hill, R., Brown, C. M., Campbell, D. A., Doblin, M. A., & Ralph, P. J. (2010). Rapid photoprotection in sea-ice diatoms from the East Antarctic pack ice. *Limnology and Oceanography*, *55*(3), 1400–1407. https://doi.org/10.4319/lo.2010.55.3.1400

Price, N. M. (2005). The elemental stoichiometry and composition of an iron-limited diatom. *Limnology and Oceanography*, *50*(4), 1159–1171. https://doi.org/10.4319/lo.2005.50.4.1159

R Core Team. (2013). *R: A language and environment for statistical computing*. Vienna, Austria: R. C. Team.

Raiswell, R., Hawkings, J., Eisenousy, A., Death, R., Tranter, M., & Wadham, J. (2018). Iron in glacial systems: Speciation, reactivity, freezing behavior, and alteration during transport. *Frontiers in Earth Science*, *6*. https://doi.org/10.3389/feart.2018.00222

Ralph, P. J., Ryan, K. G., Martin, A., & Fenton, G. (2007). Melting out of sea ice causes greater photosynthetic stress in algae than freezing in. *Journal of Phycology*, *43*(5), 948–956. https://doi.org/10.1111/j.1529-8817.2007.00382.x

Ravanelli, M., Tubertini, O., Valcher, S., & Martinotti, W. (1997). Heavy metal distribution in sediment cores from Western Ross Sea (Antarctica). *Water Air and Soil Pollution*, *99*(1–4), 697–704. https://doi.org/10.1007/Bf02406909

Redfield, A. C., Ketchum, & B. H. (1963). The influence of organisms on the composition of sea water. In M. N. Hill (Ed.), *The sea, Interscience*, 2, 26–77). New York, NY: Interscience Publishers.

Rees, C., Pender, L., Sherrin, K., Schwanger, C., Hughes, P., Tibben, S., et al. (2018). Methods for reproducible shipboard SFA nutrient measurement using RMNS and automated data processing. *Limnolology. Oceanography: Methods*, *17*(1), 25–41. https://doi.org/10.1002/lom3.10294

Rignot, E., Mouginot, J., Scheuchl, B., van den Broeke, M., van Wessem, M. J., & Morlighem, M. (2019). Four decades of Antarctic ice sheet mass balance from 1979–2017. *Proceedings of the National Academy of Sciences*, *116*(4), 1095–1103. https://doi.org/10.1073/pnas.1812883116

Rintala, J. M., Piiparinen, J., Blomster, J., Majaneva, M., Muller, S., Uusikivi, J., & Autio, R. (2014). Fast direct melting of brackish sea-ice samples results in biologically more accurate results than slow buffered melting. *Polar Biology*, *37*(12), 1811–1822. https://doi.org/10.1007/s00300-014-1563-1v

Rintoul, S. R., Chown, S. L., DeConto, R. M., England, M. H., Fricker, H. A., Masson-Delmotte, V., et al. (2018). Choosing the future of Antarctica. *Nature*, *558*(7709), 233–241. https://doi.org/10.1038/s41586-018-0173-4

Rintoul, S. R., Silvano, A., Pena-Molino, B., van Wijk, E., Rosenberg, M., Greenbaum, J. S., & Blankenship, D. D. (2016). Ocean heat drives rapid basal melt of the Totten Ice Shelf. *Science Advances*, *2*(12), e1601610. https://doi.org/10.1126/sciadv.1601610

Ryan, K. G., Ralph, P., & McMinn, A. (2004). Acclimation of Antarctic bottom-ice algal communities to lowered salinities during melting. *Polar Biology*, *27*(11), 679–686. https://doi.org/10.1007/s00300-004-0636-y

Rysgaard, S., & Glud, R. N. (2004). Anaerobic N_2 production in Arctic sea ice. *Limnology and Oceanography*, *49*(1), 86–94. https://doi.org/10.4319/lo.2004.49.1.0086

Saenz, B. T., & Arrigo, K. R. (2014). Annual primary production in Antarctic sea ice during 2005-2006 from a sea ice state estimate. *Journal of Geophysical Research: Oceans*, *119*(6), 3645–3678. https://doi.org/10.1002/2013jc009677

Schoffman, H., Lis, H., Shaked, Y., & Keren, N. (2016). Iron-nutrient interactions within phytoplankton. *Frontiers in Plant Science*, *7*, 1223. https://doi.org/10.3389/fpls.2016.01223

Sedwick, P. N., DiTullio, G. R., & Mackey, D. J. (2000). Iron and manganese in the Ross Sea, Antarctica: Seasonal iron limitation in Antarctic shelf waters. *Journal of Geophysical Research*, *105*(C5), 11321–11336. https://doi.org/10.1029/2000jc000256

Sedwick, P. N., Edwards, P. R., Mackey, D. J., Griffiths, F. B., & Parslow, J. S. (1997). Iron and manganese in surface waters of the Australian subantarctic region. *Deep-Sea Research Part I: Oceanographic Research Papers*, *44*(7), 1239–1253. https://doi.org/10.1016/S0967-0637(97)00021-6

Sedwick, P. N., Marsay, C. M., Sohst, B. M., Aguilar-Islas, A. M., Lohan, M. C., Long, M. C., et al. (2011). Early season depletion of dissolved iron in the Ross Sea polynya: Implications for iron dynamics on the Antarctic continental shelf. *Journal of Geophysical Research-Oceans*, *116*(C12). https://doi.org/10.1029/2010jc006553

Shoenfelt, E. M., Sun, J., Winckler, G., Kaplan, M. R., Borunda, A. L., Farrell, K. R., et al. (2017). High particulate iron(II) content in glacially sourced dusts enhances productivity of a model diatom. *Science Advances*, *3*(6), e1700314. https://doi.org/10.1126/sciadv.1700314

Silvano, A., Rintoul, S. R., Pena-Molino, B., Hobbs, W. R., van Wijk, E., Aoki, S., et al. (2018). Freshening by glacial meltwater enhances melting of ice shelves and reduces formation of Antarctic Bottom Water. *Science Advances*, *4*(4), eaap9467. https://doi.org/10.1126/sciadv.aap9467

Silvano, A., Rintoul, S. R., Pena-Molino, B., & Williams, G. D. (2017). Distribution of water masses and meltwater on the continental shelf near the Totten and Moscow University ice shelves. *Journal of Geophysical Research: Oceans*, *122*(3), 2050–2068. https://doi.org/10.1002/2016jc012115

Smetacek, V., Scharek, R., Gordon, L. I., Eicken, H., Fahrbach, E., Rohardt, G., & Moore, S. (1992). Early spring phytoplankton blooms in ice platelet layers of the Southern Weddell Sea, Antarctica. *Deep-Sea Research Part A, Oceanographic Research Papers*, *39*(2a), 153–168. https://doi.org/10.1016/0198-0149(92)90102-Y

Stewart, F. J., & Fritsen, C. H. (2004). Bacteria-algae relationships in Antarctic sea ice. *Antarctic Science*, *16*(2), 143–156. https://doi.org/10.1017/S0954102004001889

Sulzberger, B., Suter, D., Siffert, C., Banwart, S., & Stumm, W. (1989). Dissolution of Fe(III)(hydr)oxides in natural-waters—Laboratory assessment on the kinetics controlled by surface coordination. *Marine Chemistry*, *28*(1–3), 127–144. https://doi.org/10.1016/0304-4203(89)90191-6

Sunda, W. G. (2012). Feedback interactions between trace metal nutrients and phytoplankton in the ocean. *Frontiers of Microbiology*, *3*, 204. https://doi.org/10.3389/fmicb.2012.00204

Tagliabue, A., Bopp, L., Aumont, O., & Arrigo, K. R. (2009). Influence of light and temperature on the marine iron cycle: From theoretical to global modeling. *Global Biogeochemical Cycles*, *23*(2). https://doi.org/10.1029/2008gb003214

Taylor, S. R. M., & McLennan, S. (1985). The continental crust: Its composition and evolution . In Geoscience Texts (Vol. , pp. 1–312). Oxford: Blackwell Scientific.

Thomas, D., & Dieckmann, G. (2010). *Sea ice*, 2nd Edition, Oxford, U.K.: . Wiley-Blackwell. https://doi.org/10.1002/9781444317145

Timmermans, K. R., van der Wagt, B., & de Baar, H. J. W. (2004). Growth rates, half-saturation constants, and silicate, nitrate, and phosphate depletion in relation to iron availability of four large, open-ocean diatoms from the Southern Ocean. *Limnology and Oceanography*, *49*(6), 2141–2151. https://doi.org/10.4319/lo.2004.49.6.2141

Tison, J. L., Lorrain, R. D., Bouzette, A., Dini, M., Bondesan, A., & Stiévenard, M. (1998). Linking landfast sea ice variability to marine ice accretion at Hell Gate Ice Shelf, Ross Sea. *Antarctic Research Series*, *74*, 375–407.

Tison, J. L., Worby, A., Delille, B., Brabant, F., Papadimitriou, S., Thomas, D., et al. (2008). Temporal evolution of decaying summer first-year sea ice in the Western Weddell Sea, Antarctica. *Deep-Sea Research Part II, Topical Studies in Oceanography*, *55*(8–9), 975–987. https://doi.org/10.1016/j.dsr2.2007.12.021

Torstensson, A., Fransson, A., Currie, K., Wulff, A., & Chierici, M. (2018). Microalgal photophysiology and macronutrient distribution in summer sea ice in the Amundsen and Ross Seas, Antarctica. *PLoS One*, *13*(4), e0195587. https://doi.org/10.1371/journal.pone.0195587

Treverrow, A., Warner, R. C., Budd, W. F., & Craven, M. (2010). Meteoric and marine ice crystal orientation fabrics from the Amery Ice Shelf, East Antarctica. *Journal of Glaciology*, *56*(199), 877–890. https://doi.org/10.3189/002214310794457353

Underwood, G. J. C., Fietz, S., Papadimitriou, S., Thomas, D. N., & Dieckmann, G. S. (2010). Distribution and composition of dissolved extracellular polymeric substances (EPS) in Antarctic sea ice. *Marine Ecology Progress Series*, *404*, 1–19. https://doi.org/10.3354/meps08557

van der Linden, F. C., Tison, J. L., Champenois, W., Moreau, S., Carnat, G., Kotovitch, M., et al. (2020). Sea ice CO2 dynamics across seasons: Impact of processes at the Interfaces. *Journal of Geophysical Research: Oceans*, *125*(6). https://doi.org/10.1029/2019jc015807e2019JC015807

van der Merwe, P., Lannuzel, D., Bowie, A. R., Mancuso Nichols, C. A., & Meiners, K. M. (2011). Iron fractionation in pack and fast ice in East Antarctica: Temporal decoupling between the release of dissolved and particulate iron during spring melt. *Deep Sea Research Part II: Topical Studies in Oceanography*, *58*(9–10), 1222–1236. https://doi.org/10.1016/j.dsr2.2010.10.036

van der Merwe, P., Lannuzel, D., Bowie, A. R., & Meiners, K. M. (2011). High temporal resolution observations of spring fast ice melt and seawater iron enrichment in East Antarctica. *Journal of Geophysical Research*, *116*(G3). https://doi.org/10.1029/2010jg001628

van der Merwe, P., Lannuzel, D., Nichols, C. A. M., Meiners, K., Heil, P., Norman, L., et al. (2009). Biogeochemical observations during the winter–spring transition in East Antarctic sea ice: Evidence of iron and exopolysaccharide controls. *Marine Chemistry*, *115*(3–4), 163–175. https://doi.org/10.1016/j.marchem.2009.08.001

van der Merwe, P., Wuttig, K., Holmes, T., Trull, T. W., Chase, Z., Townsend, A. T., et al. (2019). High lability Fe particles sourced from glacial erosion can meet previously unaccounted biological demand: Heard Island, Southern Ocean. *Frontiers in Marine Science*, *6*. https://doi.org/10.3389/fmars.2019.00332

Wadham, J. L., Tranter, M., Skidmore, M., Hodson, A. J., Priscu, J., Lyons, W. B., et al. (2010). Biogeochemical weathering under ice: Size matters. *Global Biogeochemical Cycles*, *24*(3). https://doi.org/10.1029/2009gb003688

Wuttig, K., Townsend, A. T., van der Merwe, P., Gault-Ringold, M., Holmes, T., Schallenberg, C., et al. (2019). Critical evaluation of a seaFAST system for the analysis of trace metals in marine samples. *Talanta*, *197*, 653–668. https://doi.org/10.1016/j.talanta.2019.01.047

Zhou, X., Li, S., Morris, K., & Jeffries, M. O. (2007). Albedo of summer snow on sea ice, Ross Sea, Antarctica. *Journal of Geophysical Research*, *112*(D16). https://doi.org/10.1029/2006jd007907

Tagliabue A., Arrigo K. R. (2006). Processes governing the supply of iron to phytoplankton in stratified seas. *Journal of Geophysical Research*, *111*, (C6), http://dx.doi.org/10.1029/2005jc003363.